RSC Advances

This is an *Accepted Manuscript*, which has been through the Royal Society of Chemistry peer review process and has been accepted for publication.

Accepted Manuscripts are published online shortly after acceptance, before technical editing, formatting and proof reading. Using this free service, authors can make their results available to the community, in citable form, before we publish the edited article. This *Accepted Manuscript* will be replaced by the edited, formatted and paginated article as soon as this is available.

You can find more information about *Accepted Manuscripts* in the Information for Authors.

Please note that technical editing may introduce minor changes to the text and/or graphics, which may alter content. The journal's standard Terms & Conditions and the Ethical guidelines still apply. In no event shall the Royal Society of Chemistry be held responsible for any errors or omissions in this *Accepted Manuscript* or any consequences arising from the use of any information it contains.

ROYAL SOCIETY OF CHEMISTRY

www.rsc.org/advances

Assembly of Evenly Distributed Au Nanoparticles on Thiolated Reduced Graphene Oxide as an Active and Robust Catalyst for Hydrogenation of 4-Nitroarene

*Wenjun Liu, Dengrong Sun, Jinlong Fu, Rusheng Yuan, Zhaohui Li**

Research Institute of Photocatalysis, State Key Laboratory of Photocatalysis on Energy and Environment, College of Chemistry and Chemical Engineering, Fuzhou University, Fuzhou 350002, P. R. China

RSC Advances Accepted Manuscript

* Author to whom all correspondences should be addressed.

E-mail: zhaohuili1969@yahoo.com, Tel (Fax): 86-591-83779260

Abstract

Thiol-functionalized reduced graphene oxide (SRG) was prepared by coupling the carboxyl group on the pre-carboxyl-functionalized graphene oxide (GO) with cysteamine through amide bond. The as-prepared SRG can function both as a support and reducing agent for the formation of Au/SRG nanohybrid with evenly distributed Au nanoparticles on RGO. The thiol linkage on the RGO can act as anchor for Au nanoparticles and due to the existence of the strong interaction between them, the agglomeration of Au nanoparticles can be significantly impeded. The step-by-step assembly process of Au/SRG nanohybrid was monitored and the products obtained were characterized by Fourier transform infrared spectroscopy (FT-IR), Raman spectroscopy, X-ray photoelectron spectroscopy (XPS), X-ray absorption near-edge spectroscopy (XANES), atomic force microscopy (AFM), powder X-ray diffraction (XRD), transmission electron microscopy (TEM) and high-resolution transmission electron microscopy (HRTEM). The as-prepared Au/SRG nanohybrid showed superior catalytic performance for the hydrogenation of 4-nitrophenol (4-NP) to 4-aminophenol (4-AP). It is expected that the method in the preparation of Au/SRG nanohybrid can also be applied to the preparations of other RGO-based nanohybrid materials which may find a variety of interesting applications.

RSC Advances Accepted Manuscript

1. Introduction

Gold was considered for a long time to be catalytically inactive.[1] However, ever since the pioneering work by Bond, Hutchings, Haruta, Prati and Rossi, the catalysis based on Au nanoparticles have attracted extensive research interest.[2-5] Gold nanoparticles have been reported to be very active catalyst for a variety of chemical transformations, such as diverse selective oxidations of hydrocarbons,[6-8] selective hydrogenation,[9-12] low-temperature CO oxidation,[13, 14] additions to multiple C-C bonds[15] and so on. Since Au nanoparticles easily aggregate due to their high surface energy, they are usually anchored on a variety of supports for heterogeneous catalysis, including polymers, metal oxides, carbon materials, etc.[16-21] Although there still has much controversy concerning the nature of the active sites of gold nanoparticles catalysts, it has been accepted that the size, dispersion level of the nanoparticles, the interaction between Au nanoparticles and the support are the key parameters determining the performance of the supported Au nanoparticles.

Carbon-based nanomaterials such as carbon nanotubes, graphene and mesoporous carbon are important supports for the metal nanoparticles in heterogeneous catalysis.[22-26] Among them, graphene, a novel one-atom-thick two-dimensional graphitic carbon system, has attracted particular research interest due to its high surface area, excellent mechanical, thermal and electrical properties.[27-34] Although the anchoring of metal nanoparticles on the pristine graphene is difficult, reduced graphene oxide (RGO) which contains different oxygen groups directly bound to the carbon skeleton of a two-dimensional graphene-derived backbone is an ideal support for anchoring the metal nanoparticles. The surface oxygen functionalities in RGO can serve as reactive sites for the direct nucleation and growth of metal nanoparticles on the RGO surface. However, due to the unevenly distribution of these oxygen functionalities at the surface, the dispersion of the thus prepared metal nanoparticles at the graphene surface are not even.[35] To achieve a better distribution of metal nanoparticles, both non-covalent and covalent methods have been applied in the modification of the RGO surface. For example, polymers like PVP, PDDA and so on have been used to modify the graphene surface through electrostatic forces for deposition of Ag, Au and other noble metal nanoparticles.[36, 37] Chemical modifications on the RGO surface have also been carried out by different reaction types, e.g., electrophilic substitution, nucleophilic substitution, condensation and addition.[38-40] The covalent functionalizations on RGO allow the introduction of a wide

RSC Advances Accepted Manuscript

range of functional groups at the surface which can provide stronger bonding to metal nanoparticles by organic linkers and also prevent the agglomeration of the nanoparticles. For example, it has been reported that thiol group on the support can boost up the interaction between support and Au nanoparticles due to the good stability of the Au–S bond.

In this manuscript, a step-by-step method has been developed to prepare evenly distributed Au nanoparticles at surface thiol-functionalized RGO. Thiol-functionalized RGO was prepared by coupling the carboxyl group on the pre-carboxyl-functionalized graphene oxide surface with the amine group in cysteamine by the condensation agent N,N-dicyclohexylcarbodiimide (DCC). Although this coupling method to form the thiol functionalized surface has been widely used on carbon nanotubes,[41, 42] it application in the preparation of thiol functionalized RGO surface is limited.[43] The as-formed thiol functionality on the surface of RGO can further be utilized as a reducing agent to reduce $AuCl_4^-$ and the existence of the strong Au-S interaction results in the formation of well-dispersed Au nanoparticles at RGO surface. The as-prepared Au/SRG nanohybrid shows superior catalytic performance for the selective hydrogenation of 4-nitrophenol (4-NP) to the corresponding 4-aminophenol (4-AP). Moreover, the catalyst can easily be separated from the reaction mixture through phase separation and simple filtration for recycling. The step-by-step method in the preparation of Au/SRG nanohybrid is expected to be applied to the preparations of other RGO-supported noble metal nanoparticles with good distribution, uniform particle size and superior catalytic activity.

2. Experimental section

2.1. Materials. Graphite flake (99.8%, 325 mesh) was provides by Alfa. Chloroacetic acid and cysteamine were provided by Aladdin. N,N-dicyclohexylcarbodiimide (DCC) and anhydrous N,N-dimethylformamide (DMF) were purchased from Sigma Aldrich. All the reagents were used without further purifications.

2.2. Preparations

Graphene oxide (GO). GO was prepared from graphite flake by a modified Hummers method.[44] In brief, the graphite flake and $NaNO_3$ were added to cooled 98 wt% H_2SO_4 under stirring, followed by a gradual addition of $KMnO_4$. The mixture was continuously stirring at room temperature for 5 days. After that, the reaction was diluted by slow addition of H_2O and terminated by addition of 30% H_2O_2 solution. The product was collected by centrifugation and washed repeatedly with diluted HCl.

RSC Advances Accepted Manuscript

The resultant GO was suspended in water to give a brown dispersion and subjected to dialysis to completely remove the residual salts and acids.

Carboxyl-functionalized graphene oxide (GO-COOH). GO-COOH was prepared following a modified method reported by Sun et al..[45] 1.2 g of NaOH and 1.0 g of chloroacetic acid were added to a GO suspension. The mixture was then sonicated for 3 h to convert the hydroxyl groups to carboxyl groups. This was followed by neutralizing the solution. After purifying the products by repeated rinsing and filtrations, the resulting GO-COOH was collected for further use.

Thiol-functionalized reduced graphene oxide (SRG). In the thiolation reaction, the carboxyl groups in GO was coupled to the amido groups of cysteamine through amidation. An anhydrous DMF solution containing GO-COOH was mixed with 1 M DCC and a stoichiometric amount of cysteamine in ice-bath. The mixture was sonicated for 1 h and then stirred for 24 h under a nitrogen atmosphere. The resultant SRG was washed with ethanol, filtered and then dried.

Au decorated thiol-functionalized reduced graphene oxide (Au/SRG). 50 μL of 1 wt% $HAuCl_4$ aqueous solution was added to 20 mL of SRG dispersion solution under stirring. After 1 h, the resulting product was collected by centrifugation and washed several times with pure water.

Thiol-capped Au nanoparticles. The thiol-capped Au nanoparticles were prepared according to a literature method.[46] 100 mL of 0.10 M cysteamine was added to 1mg/mL aqueous metal chloride solution ($HAuCl_4 \cdot 3H_2O$, 200μL). After stirring for 20 min at R.T., 0.01 mL of 10 mM $NaBH_4$ was added, and the mixture was vigorously stirred in the dark. After 30 min, the product was collected by centrifugation, washed with Milli-Q water three times, and finally re-dispersed in 20 mL water. The Au nanoparticles suspension has a light gray color with the maximum absorption at 540 nm.

2.3. Characterizations

Fourier transform infrared spectroscopy were recorded in transmittance mode with a resolution of 4 cm^{-1} using a Nicolet Nexus 670 FTIR spectrometer. Powder X-ray diffraction (XRD) data were collected using a Bruker D8 Advance X-ray diffractometer (Cu-$K\alpha_1$ irradiation, λ = 1.5406 Å). Atomic force microscopy (AFM) image was obtained using an Auto-Probe CP/MT scanning probe microscope (XE-100(PSIA). X-ray photoelectron spectroscopy (XPS) measurements were

RSC Advances Accepted Manuscript

performed on a PHI Quantum 2000 XPS system with a monochromatic Al K_α source and a charge neutralizer. All the binding energies were referred to the C 1s peak at 284.8 eV of the surface adventitious carbon. Raman spectroscopy was performed using an invia-Reflex Micro-Raman Spectroscopy system (Renishaw Co.) with 532 nm line of an Ar ion laser at room temperature. The X-ray absorption near-edge spectroscopy (XANES) was collected in Shanghai Synchrotron Radiation Facility (SSRF) with a Si (311) double-crystal monochromator in fluorescence mode. The source of BL14W1 is a 38-pole wiggler device with maximum magnetic field 1.2 T and magnet period 80 mm. The storage ring was operated at 3.5 GeV with injection currents of 100 mA. The transmission electron microscopy (TEM) and high-resolution transmission electron microscopy (HRTEM) images were measured by a JEOL model JEM 2010 EX instrument at an accelerating voltage of 200 kV. The powder particles were supported on a carbon film coated on a 3 mm diameter fine-mesh copper grid. A suspension of the sample in ethanol was sonicated and a drop was dripped on the support film.

2.4. Catalytic experiments

To study the catalytic activity, 20 mg catalyst was dispersed in 20 mL 1 mM of 4-nitrophenol aqueous solution at room temperature. Then a freshly prepared equeous solution of 0.4 mL 2 M $NaBH_4$ was added. The reduction performing in the at 1 min intervals was monitored by the UV-vis absorption spectra in the range of 250-550 nm.

3. Results and discussion

The step-by-step assembly of the Au/SRG nanohybrid through a covalent thiol linkage is shown in scheme 1. The first step in the preparation involves the chemical oxidation and exfoliation of graphite to graphene oxide (GO) sheets by the modified Hummer's method. The successful formation of exfoliated GO has been confirmed from both the XRD and AFM measurements. As shown in Fig. 1a, after oxidation, the sample shows a well-defined diffraction peak at $2\theta = 10.2^o$, indicative of good layer regularity with a repeating interlayer distance of 0.80 nm. Instead, the original diffraction peak at 2θ of 26.2^o corresponding to (002) plane of graphite disappears. The AFM of the sample reveals that the dimension of the resultant GO sample is ca. 2 μm and has a topographic height of about 0.8 nm, indicating that the resultant sample has a single-layer structure (Fig. 2).

The second step is the carboxylation of the single-layer GO by chloroacetic acid to convert the surface epoxide and hydroxyl groups to carboxylic acid (-COOH)

RSC Advances Accepted Manuscript

moieties. The FT-IR spectra of the resultant GO-COOH shows peaks at 1712 cm^{-1} and 1570 cm^{-1}, corresponding to the surface C=O from carboxyl group and C=C respectively (Fig. 3b).[45] As compared to that of the original GO, the peak at 1712 cm^{-1} significantly increases, while the peaks at 1349 cm^{-1} and 1055 cm^{-1} which correspond to the -OH and C–O moieties on the surface decrease obviously (Fig. 3a). This indicates that the surface hydroxyl and epoxide groups on surface of the original GO have been successfully transformed to the carboxyl group during this process. The Raman spectrum of the resultant GO-COOH shows typical D band at 1352 cm^{-1} and G band at 1592 cm^{-1}, corresponding to the breathing mode of sp^2 carbon and graphitic sp^2-bonded carbon respectively.[47] The intensity ratio of D and G band (I_D/I_G ratio) for the resultant GO-COOH is determined to be 0.95, comparable to that observed over the original GO (I_D/I_G=0.96) (Fig. 4a and b). Since the ratio of I_D/I_G is an indicator for the extent of defects in the graphene-based materials, the comparable I_D/I_G ratio observed over GO-COOH and the original GO suggests that the carboxylation process does not induce defects in the resultant GO-COOH.

To prepare the thiol functionalized reduced grapheme oxide, the condensation agent DCC was used to couple the carboxyl group on the GO-COOH surface with the amine group in cysteamine. DCC has been widely used in the formation of polypeptide from the condensation of amino acids. Recently, the application of DCC as the dehydration agent in the formation of amides from amine and carboxyl acids under mild condition has also been reported.[41] The FTIR spectrum of the resultant thiol functionalized SRG shows typical amide I band at 1650 cm^{-1} and amide II band at 1517 cm^{-1} respectively,[43, 45] which confirms the formation of the amide bond between the surface carboxyl groups and amine group in cysteamine (Fig. 3c).

The formation of amide bond has also been confirmed by the XPS spectra. As shown in Fig. 5a, the XPS in the N1s region shows peaks at 400.1 eV, in agreement with the binding energy of the nitrogen in amide bond.[42] The XPS spectra in the S 2p region show peaks at 163.9 and 165 eV, corresponding to the S $2p_{3/2}$ and S $2p_{1/2}$, a confirmation that the sample is surface functionalized with thiol group (Fig. 5b). The peak in the O 1s region in XPS spectrum can be deconvoluted to 531.1 eV, 532.0 eV and 533.5 eV, which can be assigned to C=O, C-O and O-H respectively (Fig. 5c). As compared to original GO, the peak of O-H has dramatically decreased due to carboxylation of the single-layer GO. Similarly, the C 1s peaks can also be deconvoluted to peaks at 284.6, 285.2, 286.3 and 288.4 eV, assigned to C=C, C-S or

RSC Advances Accepted Manuscript

C-N, C-O and C=O, repectively (Fig. 5d). The reduction degree of GO defined as the ratio of oxygen-bound carbon content in GO has also been determined based on the XPS results following the equation:

$$\text{O-bound C \%} = (A_{C-O}+A_{O-C=O})/(A_{C-C}+A_{C-O}+A_{O-C=O}) \times 100\%$$

where A_{C-C}, A_{C-O}, and $A_{O-C=O}$ are the peak areas in the XPS spectra for the sp^2-hybridized (C–C) and O-bound (C–O and O–C=O) carbon, respectively.[48] It is found that after the coupling reaction, the O-bound C content decreases from the original 55% in GO to 27% in SRG, indicating that the coupling reaction also leads to partial reduction of GO. This observation is not surprising since generally the thiol is a reducing agent. The partial reduction of GO by the thiol group would inevitably generate defects in GO. This is also confirmed from the Raman result. The Raman spectra of the thiol functionalized GO show D band at 1352 cm^{-1} and G band at 1572 cm^{-1} respectively (Fig. 4c). The I_D/I_G ratio increases from the original 0.95 for GO-COOH to the 1.05 in thiol-functionalized GO, indicating that the coupling process to form the thiol functionalized GO has resulted in the increase of defects.[47] All the above characterizations indicate that cysteamine is grafted on the surface of GO-COOH through the formation of amide linkage.

Since that thiols are strong reducing agents and the strong affinity of thiol group to noble metal, especially gold, has been well documented in literature,[49,50] the addition of $HAuCl_4$ solution into the as-formed SRG is expected to form the Au nanoparticles on the SRG surface. The XRD pattern of the Au/SRG sample prepared by stirring the SRG suspension in the presence of $HAuCl_4$ for 1h shows the diffraction peaks at 2θ of 24.3°, 38.1° and 44.3° (Fig. 1c). The peak at 24.3° can be indexed to the (002) crystal face of functionalized graphene oxide, while the other two peaks can be ascribed to (111) and (200) planes of Au in face centered cubic (fcc) structure. This confirms that Au nanoparticles have been successfully obtained on the surface of SRG. The XPS spectra of Au/SRG in Au 4f region show obvious peaks at 87.7 eV and 84.0 eV, attributed to $4f_{7/2}$ and $4f_{5/2}$ of Au^0, and peaks at 88.5 eV and 84.8 eV, corresponding to $4f_{7/2}$ and $4f_{5/2}$ of Au^+ (Fig. 6a). The ratio of Au^0 to Au^+ is determined to be 24:1, indicating that most of the Au^{3+} has been reduced to Au^0. As compared to the pristine SRG, the XPS spectrum in the S 2p region can be deconvoluted into two spin-orbit doublets for S-H (163.9 and 165 eV) and S-Au (162 and 163.1 eV), which can be assigned to S bonding to gold nanoparticles and the free thiol groups,

RSC Advances Accepted Manuscript

respectively (Fig. 6b).[42] On the contrary, the XPS spectra of C 1s, O 1s and N 1s do not change obviously, suggesting that the deposition of Au nanoparticles do not significantly influence of the property of the RGO substrate (Fig. 6c-e). Similar results could be obtained from the Au L_{III}-edge X-ray absorption near-edge spectroscopy (XANES) of Au/SRG (Fig. 7). The characteristic three-peak pattern following the edge jump at about 11.919 keV indicates the presence of the Au^0 in a fcc structure.[51] As compared with that of Au foil, a slight increase of the first two peaks after the edge jump could be found, which is caused by the minority Au^+ that connected with S-H in Au/SRG. The Raman spectrum of the Au/SRG shows D band at 1352 cm^{-1} and G band at 1592 cm^{-1} with a I_D/I_G ratio of 1.04 (Fig. 4d). The comparable I_D/I_G ratio observed over Au/SRG and pristine SRG (I_D/I_G=1.05) indicates that the reduction and deposition of Au nanoparticles does not induce defects on the SRG substrate. The TEM image of Au/SRG shows clearly that Au nanoparticles are evenly deposited on the surfaces of SRG sheets (Fig. 8a). More than 90% of the Au nanoparticles fall in the size range of 15-20 nm with the mean particle diameter determined to be about 17 nm (Fig. 8c), in good agreement with that determined from the XRD result (16 nm). Clear lattice fringes of d = 0.235 nm is observed in the HRTEM image, which matches well with the (111) planes of fcc Au (Fig. 8b). The deposited Au nanoparticles can stand prolonged sonication, indicating that such a step-by-step method can lead to robust and evenly deposited Au nanoparticles on the SRG surface.

Since Au nanoparticles exhibit excellent catalytic activity for the hydrogenation, the catalytic activity of the as-prepared Au/SRG nanohybrid was evaluated by the hydrogenation of 4-nitrophenol (4-NP) in the presence of $NaBH_4$.[52] 4-Nitrophenol, which is typically found in industrial products and agricultural waste waters, is harmful and hazardous. In addition, the selective hydrogenation of 4-NP to the corresponding 4-aminophenol (4-AP) is known to be one of the fundamental reactions for the synthesis and manufacture of fine and industrial chemicals. Usually this reaction is achieved in the presence of metal nanoparticles, which can catalyze the reaction by facilitating electron relay from the donor BH_4^- to the acceptor 4-NP to overcome the kinetic barrier.[53] Since 4-NP shows a typical absorbance peak at 400 nm, the hydrogenation of 4-NP to 4-AP can decrease the intensity of the peak at 400 nm while a new absorption peak at 300 nm corresponding to 4-AP can develop. As shown in Fig. 9a, when Au/SRG was added into the solution containing 4-NP and $NaBH_4$,

RSC Advances Accepted Manuscript

the intensity of the strong absorption peak at 400 nm gradually decreased and within 4 mins, the whole peak disappeared. In the meantime, a new absorption peak at 300 nm appeared with its intensity increased gradually during this period. This indicates that in the presence of Au/SRG, $NaBH_4$ can hydrogenate 4-NP to 4-AP, and no other by-products have been observed. However, almost no decrease of the peak at 400 nm was observed over pure $NaBH_4$, suggesting that the hydrogenation of 4-NP in the presence of pure $NaBH_4$ can be neglected. Similar hydrogenation of 4-NP in the presence of support-free thiol-capped Au nanoparticles was more slowly and a complete conversion of 4-NP to 4-AP was not achieved even after 5h reaction (Fig. 9a inset). The low catalytic activity observed over the support-free thiol-capped Au is due to the aggregation of Au nanoparticles in the reaction system. Remarkably, the turnover frequency (TOF) for 4-NP hydrogenation over Au/SRG is calculated to be 60 h^{-1}, much higher than that over polygonal Au nanoparticles (0.4 h^{-1}),[54] one of conventional catalyst for 4-NP hydrogenation. Au/SRG also show enhanced activity as compared to Au nanoparticles supported on a variety of supports,[55] like PDMAEMA-PS, PNIPAP-b-P4VP, chitosan-coated iron oxide, α-cyclodextrin and graphene oxide, indicating that the thiolated RGO support plays an important role in enhancing the catalytic activity of 4-NP hydrogenation. The increase of the catalytic activity may be due to the following. (i) The thiolated RGO can act as a support for Au nanoparticles and promote the Au-mediated electron transfer from BH_4^- to 4-NP due to its high electronic conductivity; (ii) A high concentration of 4-NP can be adsorbed on the thiolated RGO via π-π stacking interactions, which is beneficial to the catalytic reaction; (iii) As compared with bare Au nanoparticles, thiolated RGO can offer an environment to prevent the aggregation of Au nanoparticles due to the existence of the Au-S bond, which can help the catalyst to maintain its long term activity.

By assuming the reaction to be pseudo-zero-order[56] which is reasonable because the concentrations of 4-nitrophenol and $NaBH_4$ largely exceeded those of the catalysts, the catalytic rate constant (k) could be determined from the curve plotted of the concentration of 4-nitrophenol C_t, ie, the absorbance *versus* reaction time (t). As shown in Fig. 9b, a good relationship can be built between C_t and t and the corresponding k calculated from the linear slope was 0.5 mM min^{-1} for Au/SRG nanohybrid.

The stability of the Au/SRG nanohybrid for the catalytic hydrogenation of 4-NP

RSC Advances Accepted Manuscript

has also been investigated. As shown in Fig. 10a, Au/SRG nanohybrid shows almost similar catalytic activity for the hydrogenation of 4-NP over five cycles of use. In addition, the catalyst after the reaction shows similar XRD patterns as that of the fresh one, indicating that the metallic state of Au is still kept (Fig. 10b inset). The TEM image of the sample after the catalytic reaction shows that Au with the same size distribution is still evenly dispersed on the surface (Fig. 10b). All these suggest that the Au/SRG nanohybrid is an active, robust and reusable catalyst for hydrogenation of 4-NP.

4. Conclusions

An efficient method in the preparation of thiol-functionalized RGO has been developed. Evenly dispersed Au nanoparticles on RGO can be obtained by using the thiol-functionalzied RGO as a reducing agent as well as a support. The thiol linkage on the RGO can act as anchor for Au nanoparticles and due to the existence of the strong interaction between them, the agglomeration of Au nanoparticles can be significantly impeded. The as-prepared Au/SRG nanohybrid shows superior catalytic activity and high stability for the selective hydrogenation of 4-NP to the corresponding 4-AP. It is expected that the step-by-step method in the preparation of Au/SRG nanohybrid can also be applied to the preparations of other RGO-based nanohybrid materials which may find a variety of interesting applications.

Acknowledgements

We are grateful to Shanghai Synchrotron Radiation Facility (SSRF) of China for the X-ray absorption near-edge spectroscopy (XANES) measurements at the BL14W1 beamline. The work was supported by 973 Programs (2014CB239303), NSFC (21273035, 21077023) and Specialized Research Fund for the Doctoral Program of Higher Education (20123514110002). Z. Li thanks the Award Program for Minjiang Scholar Professorship for financial support.

References

1. H. Schmidbaur, *Naturwiss Rundsch.*, 1995, **48**, 443-451.

2. G. C. Bond, P. A. Sermon, G. Webb, D. A. Buchanan and P. B. Wells, *J. Chem. Soc. Chem. Commun.*, 1973, 444-445.

3. G. J. Hutchings, *J. Catal.*, 1985, **96**, 292-295.

4. M. Haruta, T. Kobayashi, H. Sano and N. Yamada, *Chem. Lett.*, 1987, **16**, 405-408.

5. L. Prati and M. Rossi, *J. Catal.*, 1998, **176**, 552-560.

6. S. E. Davis, M. S. Ide and R. J. Davis, *Green Chem.*, 2013, **15**, 17-45.

RSC Advances Accepted Manuscript

7. A. Abad, C. Almela, A. Corma and H. García, *Chem. Commun.*, 2006, 3178-3180.

8. C. D. Pina, E. Falletta and M. Rossi, *Chem. Soc. Rev.*, 2012, **41**, 350-369.

9. A. Corma and P. Serna, *Science*, 2006, **313**, 332 -334.

10. M. Pan, H. C. Ham, W. Y. Yu, G. S. Hwang and C. B. Mullins, *J. Am. Chem. Soc.*, 2013, **135**, 436-442.

11. M, Pan, Z. D. Pozun, A. J. Brush, G. Henkelman and C. B. Mullins, *ChemCatChem*, 2012, **4**, 1241-1244.

12. M. Pan, A. J. Brush, Z. D. Pozun, H. C. Ham, W. Y. Yu, G. Henkelman, G. S. Hwang and C. B. Mullins, *Chem. Soc. Rev.*, 2013, **42**, 5002-5013.

13. Y. Maeda, Y. Iizuka and M. Kohyama, *J. Am. Chem. Soc.*, 2013, **135**, 906-909.

14. Z. Wu, S. Zhou, H. Zhu, S. Dai and S. H. Overbury, *J. Phys. Chem. C*, 2009, **113**, 3726-3734.

15. M. Bandini, *Chem. Soc. Rev.*, 2011, **40**, 1358-1367.

16. H. Yin, H. Tang, D. Wang, Y. Gao and Z. Tang, *ACS Nano*, 2012, **6**, 8288-8297.

17. F. Shi, Q. Zhang, Y. Ma, Y. He and Y. Deng, *J. Am. Chem. Soc.*, 2005, **127**, 4182-4183.

18. C. Y. Ma, Z. Mu, J. J. Li, Y. G. Jin, J. Cheng, G. Q. Lu, Z. P. Hao and S. Z. Qiao, *J. Am. Chem. Soc.*, 2010, **132**, 2608-2613.

19. Y. Guan and E. J. M. Hensen, *Appl. Catal. A*, 2009, **361**, 49-56.

20. Z. Wang, J. Zhang, Z. Yin, S. Wu, D. Mandler and H. Zhang, *Nanoscale*, 2012, **4**, 2728-2733.

21. Z. Zanolli, R. Leghrib, A. J. Felten, Pireaux, E. Llobet and J. C. Charlier, *ACS Nano*, 2011, **5**, 4592-4599.

22. L. Chen, K. Yang, H. Liu and X. Wang, *Carbon*, 2008, **46**, 2137-2143.

23. P. V. Kamat, *J. Phys. Chem. Lett.*, 2010, **1**, 520-527.

24. X. Huang, Z. Yin, S. Wu, X. Qi, Q. He, Q. Zhang, Q. Yan, F. Boey and H. Zhang, *Small*, 2011, **7**, 1876-1902.

25. X. Xie, J. Long, J. Xu, L. Chen, Y. Wang, Z. Zhang and X. Wang, *RSC Adv.*, 2012, **2**, 12438-12446.

26. S. Wang, Q. Zhao, H. Wei, J. Q. Wang, M. Cho, H. S. Cho, O. Terasaki and Y. Wan, *J. Am. Chem. Soc.*, 2013, **135**, 11849-11860.

27. S. Pang, Y. Hernandez, X. Feng and K. Müllen, *Adv. Mater.*, 2011, **23**, 2779-2795.

28. D. A. Dikin, S. Stankovich and E. J. Zimney, *Nature*, 2007, **448**, 457-460.

29. S. Stankovich, D. A. Dikin and G. H. B. Dommett, *Nature*, 2006, **442**, 282-286.

RSC Advances Accepted Manuscript

30. W. Wei, T. He, X. Teng, S. Wu, L. Ma, H. Zhang, J. Ma, Y. Yang, H. Chen, Y. Han, H. Sun and L. Huang, *Small.*, 2012, **8**, 2271-2276.

31. Y. Kopelevich and P. Esquinazi, *Adv. Mater.*, 2007, **19**, 4559-4563.

32. T. Schwamb, B. R. Burg, N. C. Schirmer and D. Poulikakos, *Nanotechnology*, 2009, **20**, 405704.

33. C. G. Navarro, R. T. Weitz and A. M. Bittner, *Nano Lett.*, 2007, **7**, 3499-3503.

34. Y. B. Zhang, Y. W. Tan and H. L. Stormer, *Nature*, 2005, **438**, 201–204.

35. G. Goncalves, P. A. A. P. Marques, C. M. Granadeiro, H. I. S. Nogueira, M. K. Singh and J. Gracio, *Chem. Mater.*, 2009, **21**, 4796-4802.

36. Z. Zhang, F. G. Xu, W. S. Yang, M. Y. Guo, X. D Wang, B. L. Zhang and J. L. Tang, *Chem. Commun.*, 2011, **47**, 6440-6442.

37. Y. Fang, S. Guo, C. Zhu, Y. Zhai and E. Wang, *Langmuir*, 2010, **26**, 11277-11282 .

38. J. Liu, J. Tang and J. J. Gooding, *J. Mater. Chem.*, 2012, **22**, 12435-12452.

39. H. Yao, L. Jin, H. J. Sue, Y. Sumi and R. Nishimura, *J. Mater. Chem. A*, 2013, **1**, 10783-10789.

40. D. Marquardt, F. Beckert, F. Pennetreau, F. Tölle, R. Mülhaupt, O. Riant, S. Hermans, J. Barthel and C. Janiak, *Carbon*, 2014, **66**, 285-294.

41. S. Park, H. R. Kim, J. Kim, C. Jung, C. K. Rhee, K. Kwon and Y. Kim, *Carbon*, 2011, **49**, 487-494.

42. L. Minati, G. Speranza, S. Torrengo, L. Toniutti, C. Migliaresi, D. Maniglio, M. Ferrari and A. Chiasera, *Surface Science*, 2010, **604**, 1414–1419.

43. E. S. Orth, J. E. S. Fonsaca, S. H. Domingues, H. Mehl, M. M. Oliveirab and A. J. G. Zarbin, *Carbon*, 2013, **61**, 543-550.

44. A. Lerf, H. Y. He and M. Forster, *J. Phys. Chem. B*, 1998, **102**, 4477-4482.

45. X. M. Sun, Z. Liu, K. Welsher, J. T. Robinson, A. Goodwin, S. Zaric and H. J. Dai, *Nano Res*, 2008, **1**, 203-212.

46. S. N. Sarangi, A. M. P. Hussain, S. N. Sahu, *Appl. Phys. Lett.*, 2009, **95**, 73109.

47. C. K. Chua and M. Pumera, *Chem. Eur. J.*, 2013, **19**, 2005-2011.

48. A. Iwase, Y. H. Ng, Y. Ishiguro, A. Kudo and R. Amal, *J. Am. Chem. Soc.*, 2011, **133**, 11054-11057.

49. N. R. Jana and X. Peng, *J. Am. Chem. Soc.*, 2003, **125**, 14280-14281.

50. C. Yang, G. An and X. Zhao, *J Mater Sci: Mater Electron*, 2013, **24**, 3490-3495.

51. P. Zhang, X. Zhou, Y. Tang and T. K. Sham, *Langmuir*, 2005, **21**, 8502-8508.

RSC Advances Accepted Manuscript

52. Y. Choi, H. S. Bae, E. Seo, S. Jang, K. H. Park and B. S. Kim, *J. Mater. Chem.* 2011, **21**, 15431-15436.

53. J. Huang, L. M. Zhang, B. Chen, N. Ji, F. H. Chen, Y. Zhang and Z. J. Zhang, *Nanoscale*, 2010, **2**, 2733-2738.

54. M. H. Rashid and T. K. Mandal, *Adv. Funct. Mater.*, 2008, **18**, 2261-2271.

55. K. Layek, M. L. Kantam, M. Shirai, D. N. Hamane, T. Sasaki and H. Maheswaran, *Green Chem.*, 2012, **14**, 3164-3174.

56. Y. M. Zhang, X. Yuan, Y. Wang and Y. Chen, *J. Mater. Chem.*, 2012, **22**, 7245-7251.

RSC Advances Accepted Manuscript

Captions for Figures

Fig. 1 XRD patterns for (a) GO, (b) SRG and (c) Au/SRG nanohybrid.

Fig. 2 AFM images and cross-section analysis of GO suspension obtained, deposited on freshly cleaved mica substrates.

Fig. 3 FTIR spectra of (a) GO, (b) GO-COOH, (c) SRG and (d) Au/SRG nanohybrid.

Fig. 4 Raman spectra of (a) GO, (b) GO-COOH, (c) SRG and (d) Au/SRG nanohybrid.

Fig. 5 XPS spectra in (a) N 1s region, (b) S 2p region, (c) O 1s region, (d) C 1s region and (e) survey for SRG.

Fig. 6 XPS spectra in (a) Au 4f region, (b) S 2p region, (c) C 1s region, (d) O 1s region, (e) N 1s region and (f) survey for Au/SRG nanohybrid.

Fig. 7 XAFS normalization absorption spectra for Au foil and Au/SRG.

Fig. 8 Images of Au/SRG nanohybrid (a) low magnification TEM image; (b) HRTEM image; (c) the size distribution of supported Au nanoparticles.

Fig. 9 Time dependent UV-vis absorption spectra for the catalytic hydrogenation of 4-NP by $NaBH_4$ in the presence of (a) Au/SRG nanohybrid and thiol-capped Au nanoparticles (insert). (b) Comparative plots of C_t *vs.* time for Au/SRG nanohybrid towards the hydrogenation of 4-NP by $NaBH_4$.

Fig. 10 (a) Cycling runs in the catalytic hydrogenation of 4-NP over Au/SRG nanohybrid. (b) TEM image and XRD pattern (inset) of Au/SRG nanohybrid after the catalytic cycling runs.

Scheme 1 Step-by-step assembly of Au/SRG nanohybrid.

RSC Advances Accepted Manuscript

Fig. 1

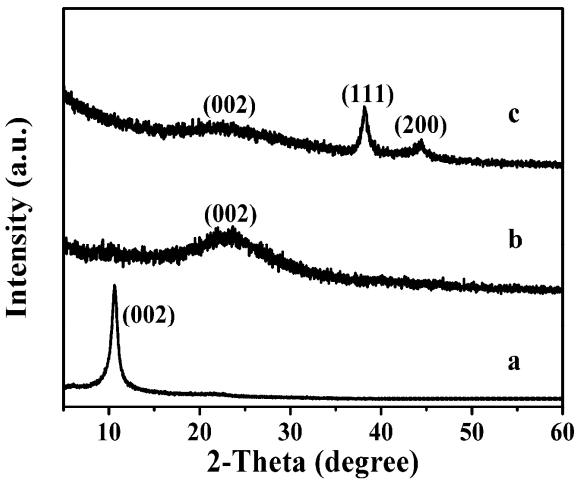

RSC Advances Accepted Manuscript

Fig. 2

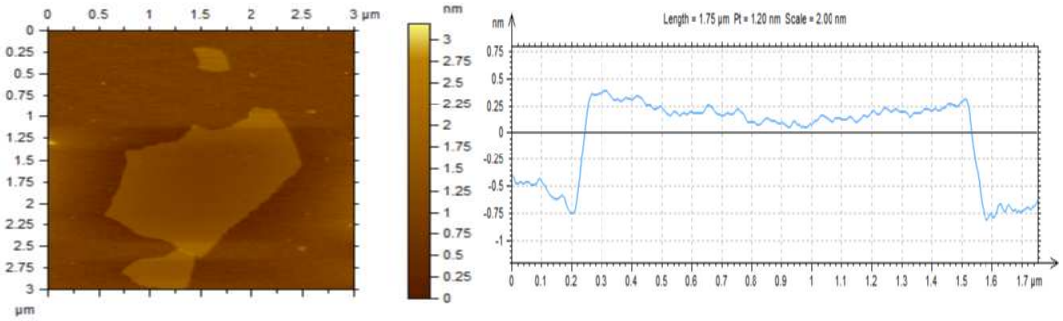

RSC Advances Accepted Manuscript

Fig. 3

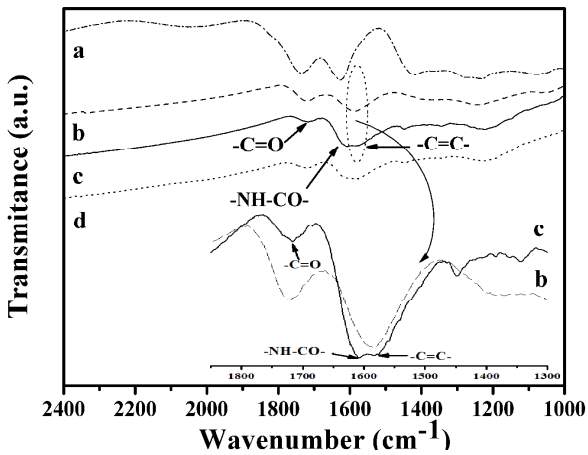

RSC Advances Accepted Manuscript

Fig. 4

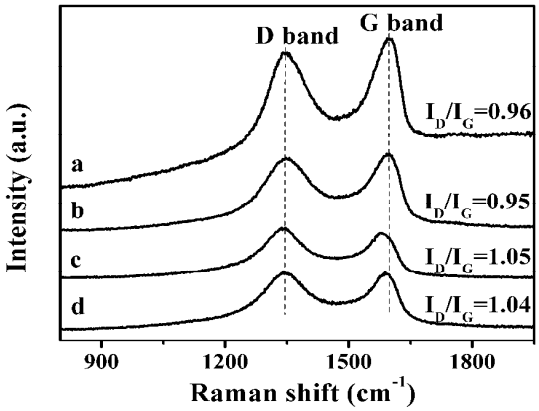

RSC Advances Accepted Manuscript

Fig. 5

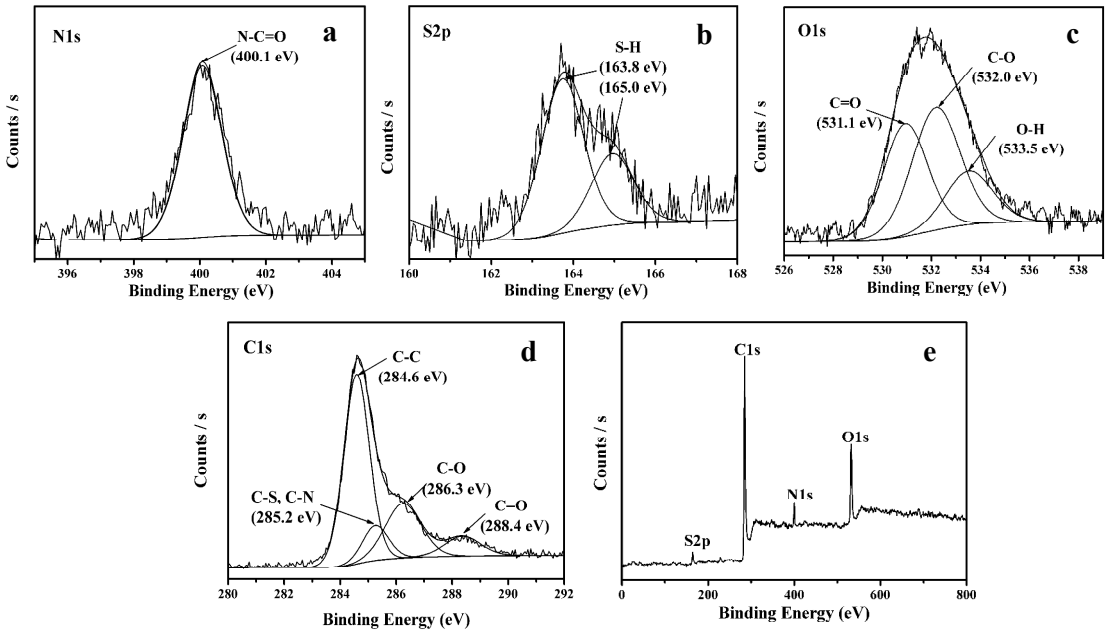

RSC Advances Accepted Manuscript

Fig. 6

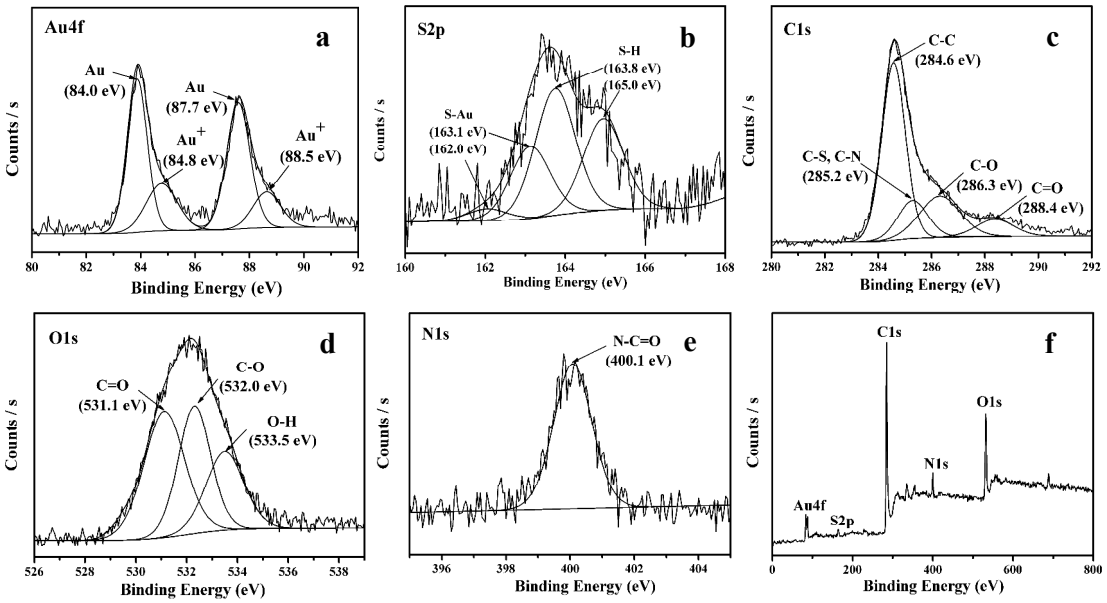

RSC Advances Accepted Manuscript

Fig. 7

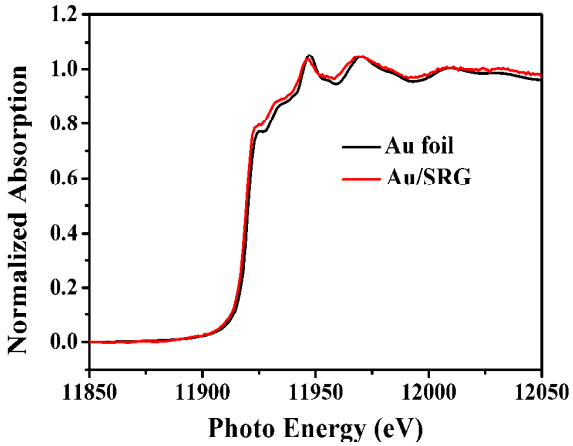

RSC Advances Accepted Manuscript

Fig. 8

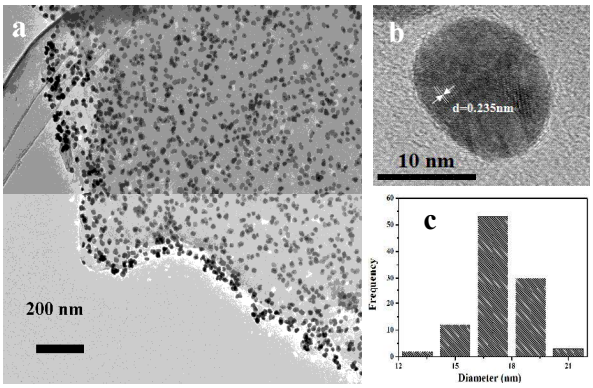

RSC Advances Accepted Manuscript

Fig. 9

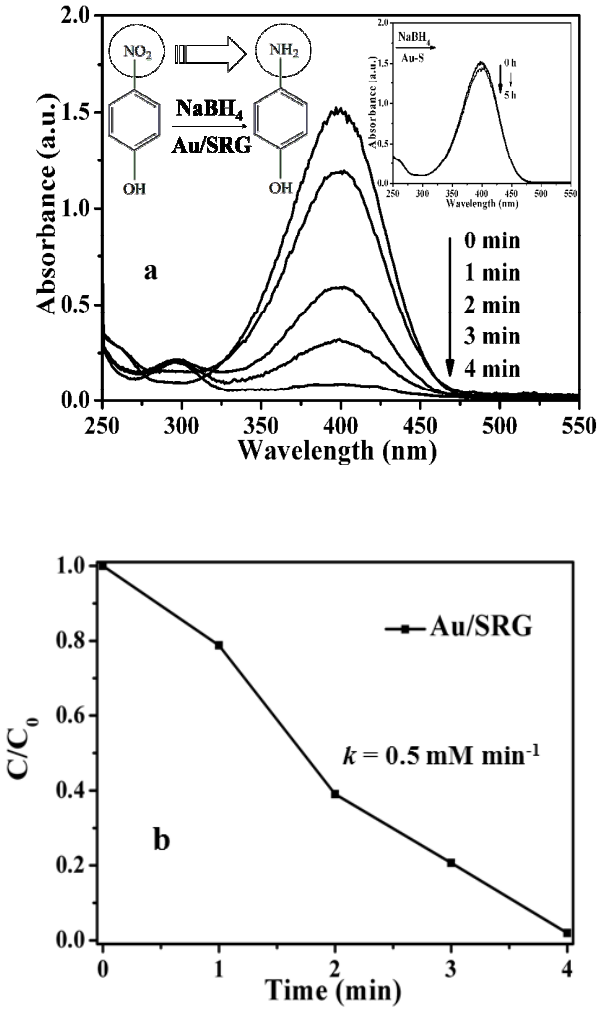

RSC Advances Accepted Manuscript

Fig. 10

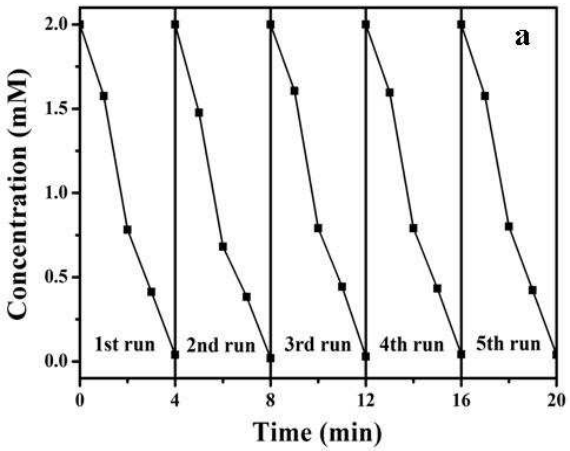

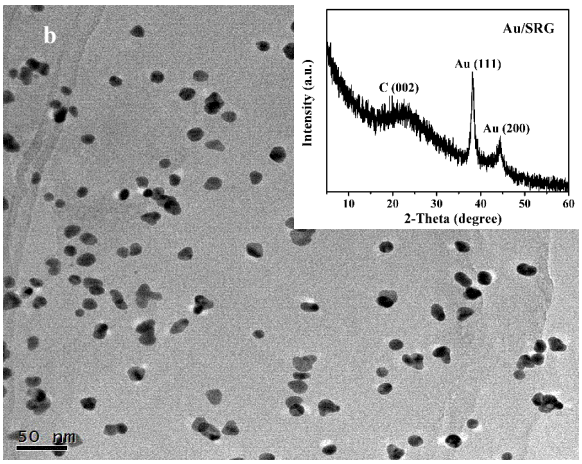

RSC Advances Accepted Manuscript

Scheme 1

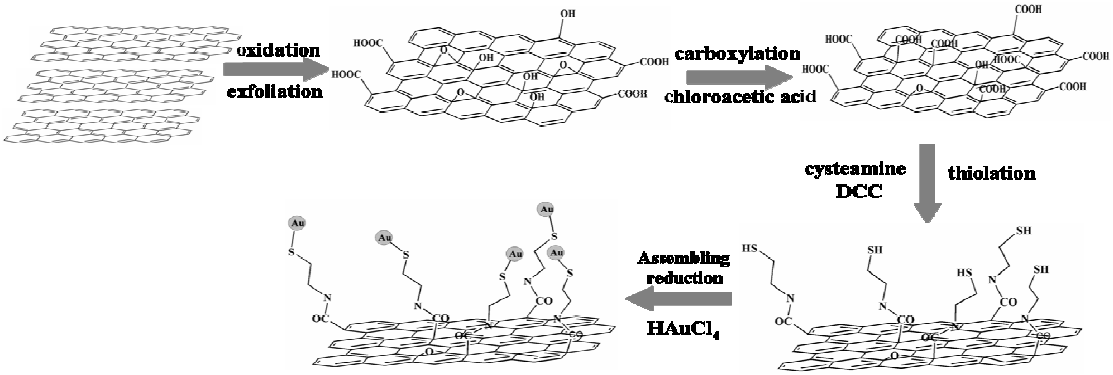

RSC Advances Accepted Manuscript

Table of content entry

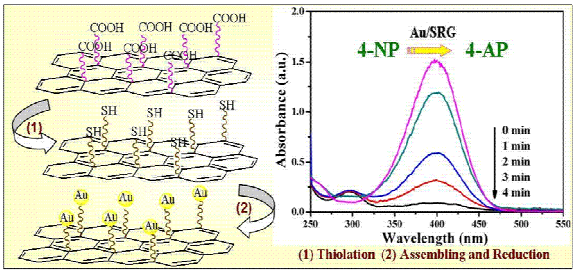

Au/SRG nanohybrid with evenly distributed Au nanoparticles anchored on reduced graphene oxide via covalent thiol linkage shows superior catalytic performance for hydrogenation of 4-nitrophenol

RSC Advances Accepted Manuscript